ACS APPLIED MATERIALS & INTERFACES

Research Article

Cite This: ACS Appl. Mater. Interfaces 2018, 10, 24627−24637

www.acsami.org

Thickness-Dependent Evolution of Piezoresponses and Stripe 90° Domains in (101)-Oriented Ferroelectric $PbTiO_3$ Thin Films

Yanpeng Feng,[†,‡] Yunlong Tang,[†] Desheng Ma,[§] Yinlian Zhu,[*,†] Minjie Zou,[†,∥] Mengjiao Han,[†,‡] Jinyuan Ma,[†,⊥] and Xiuliang Ma[†,⊥]

[†]Shenyang National Laboratory for Materials Science, Institute of Metal Research, Chinese Academy of Sciences, Wenhua Road 72, 110016 Shenyang, China

[‡]University of Chinese Academy of Sciences, Yuquan Road 19, 100049 Beijing, China

[§]School of Physics, Nankai University, Weijin Road 94, 300071 Tianjin, China

[∥]School of Material Science and Engineering, University of Science and Technology of China, 230026 Hefei, China

[⊥]School of Materials Sciences and Engineering, Lanzhou University of Technology, Langongping Road 287, 730050 Lanzhou, China

ABSTRACT: High-index ferroelectric films as (101)-oriented ones exhibit enhanced dielectric responses, piezoelectric responses, and exotic ferroelectric switching behaviors, which are potential candidates for applications in memories and capacitors. However, possible domain patterns and domain wall structures in (101)-oriented ferroelectric thin films are still elusive, which results in difficulties in understanding the origin and further modulating their special properties. In this work, a series of $PbTiO_3$ (PTO) thin films with 35, 50, 60, and 70 nm in thickness were grown on (101)-oriented $(LaAlO_3)_{0.29}(SrTa_{1/2}Al_{1/2}O_3)_{0.71}$ (LSAT(101)) substrates by pulsed laser deposition and investigated by both piezoresponse force microscopy (PFM) and (scanning) transmission electron microscopy ((S)TEM). PFM measurements reveal that periodic stripe domains are dominant in 50 nm thick PTO films. Besides stripe domains, *a*/*c* domains appear in films with thickness more than 60 nm. A thickness-dependent evolution of piezoresponse amplitude indicates that the 50 nm thick PTO films demonstrate a superior piezoresponse. Electron diffraction and contrast analysis clarify that all these (101)-oriented PTO films contain periodic stripe ferroelectric 90° domains. The domain periods increase with the film thickness following Kittel's law. Aberration-corrected STEM imaging reveals that the stripe ferroelectric 90° domains have an alternate arrangement of wide and narrow *c* domains with polarization directions along [100] for c_1 domains and $[00\bar{1}]$ for c_2 domains, forming a "head-to-tail" polarization configuration. Further strain analysis reveals that stripe domains have uniform strain distributions and distinct lattice rotations around domain walls. It is proposed that the periodic arrangement of high-density stripe 90° domains in 50 nm thick PTO films is the main contributor to the superior piezoresponse behavior. These results are expected to provide useful information to understand the domain structures in (101)-oriented PTO thin films and thus facilitate further modulation of the properties for potential applications.

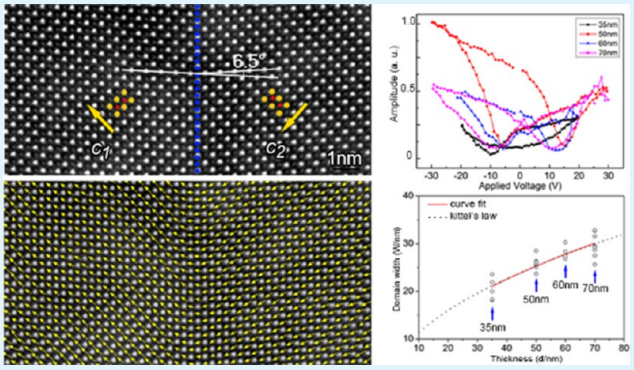

KEYWORDS: *ferroelectric thin films, $PbTiO_3$, stripe 90° domain, piezoresponse, TEM*

1. INTRODUCTION

Ferroelectrics featuring electrically switchable spontaneous polarizations have attracted much attention as potential candidates for nonvolatile ferroelectric random access memories, ultrathin ferroelectric capacitors, tunnel junction devices, and transducers.[1−4] Due to the trend of device miniaturization, ferroelectrics are commonly applied to devices in the form of thin films that have various domain configurations.[5]

The formation of domains in epitaxial ferroelectric thin films is determined by the minimization of the total free energy, including electrostatic energy, elastic strain energy, and domain wall energy of the system.[6] The resulting domain structure has a profound influence on dielectricity, piezoelectricity, and ferroelectric switching behaviors.[4] For instance, previous studies have shown that 180° nanodomains in $PbTiO_3$/$SrTiO_3$ superlattices can enhance dielectric responses, whereas the switching of 90° domains can enhance piezoelectric property in tetragonal ferroelectric thin films.[7−10] Furthermore, the domain walls, which are the interfaces of adjacent domains with different polarization directions, exhibit various exotic properties, such as domain wall conductivity and photovoltaic effect.[11−15] Thus, it is important to understand and further

Received: May 3, 2018
Accepted: July 3, 2018
Published: July 3, 2018

DOI: 10.1021/acsami.8b07206
ACS Appl. Mater. Interfaces 2018, 10, 24627−24637

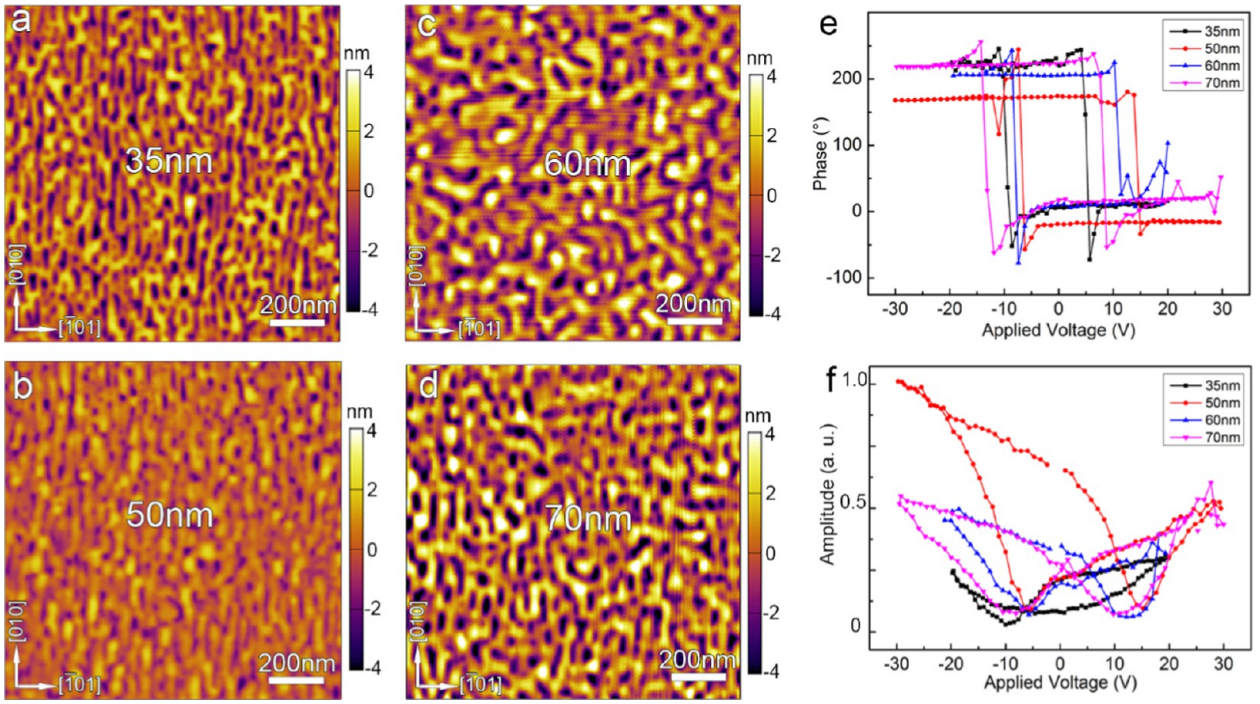

Figure 1. (a–d) Surface topographic images of PTO thin films with different thicknesses grown on LSAT(101) substrates: (a) 35 nm; (b) 50 nm; (c) 60 nm; and (d) 70 nm. (e, f) Local PFM hysteresis loops of PTO thin films with different thicknesses grown on LSAT(101) substrates. (e) Phase hysteresis loops and (f) amplitude hysteresis loops.

modulate the domain and domain wall structures at atomic scale in ferroelectric thin films.

For tetragonal ferroelectrics, such as $PbTiO_3$ (PTO), $PbZr_{0.2}Ti_{0.8}O_3$, the polarization direction is along ⟨001⟩, leading to two possible domain structures: 180° domains and 90° domains. The 90° domains also include a/c domains and a_1/a_2 domains, where c domain possesses out-of-plane polarization direction and a domain possesses in-plane polarization direction.[16,17] For decades, much attention has been on experimental observation and theoretical simulation about various domain structures in ferroelectric thin films, such as $c/a_1/a_2$ domains, bubble domains, exotic polar flux-closure domains, and polar vortices.[18−26] Both theoretical and experimental studies have indicated that the evolution of domain structures in tetragonal PTO thin films is from the c domains to $c/a_1/a_2$ domains, and then to full a_1/a_2 domains when the misfit strain changes from large compressive to large tensile strains.[18−20,27,28] It has been reported that film thickness and cooling rate also have effects on the domain structures in ferroelectric thin films.[29,30]

However, the experimental studies on the evolution of domain structures with film thickness are more challenging because of the various mismatches between different substrates and films. Despite this fact, most previous studies have revealed that the relationship between domain width (W) and film thickness (d) obeys a square root dependence ($W \propto d^{1/2}$),[20] whereas some other studies have indicated that linear or other kind of relationships are also feasible for some ferroelectric films.[22,30] Nevertheless, these studies have mainly focused on the (001)-oriented ferroelectric thin films. Experimental observations on how the domain structures evolve with film thickness or other parameters in ferroelectric films orientated in other directions have not been widely reported.[31−34] Furthermore, the scanty previous characterizations of domain structures in (101)- and (111)-oriented thin films were usually done by piezoresponse force microscope (PFM), which cannot provide atomic information of domain and domain wall structures due to the restriction of its resolution. Thus, fine analysis of the domain structures and their evolutions with film thickness in (101)- and (111)-oriented ferroelectric PTO thin films is necessary and demanded for better understanding of the domain formation rules, domain wall structures, and their impact on electric properties because theoretical simulations and experimental studies have shown that dielectric and piezoelectric responses are enhanced due to high domain wall density in single-crystal ferroelectrics with different crystallographic directions and (101)/(111)-oriented $PbZr_{0.2}Ti_{0.8}O_3$ thin films.[31,32,35,36]

In this article, we deposited [101]PTO thin films with different thicknesses on (101)-oriented $(LaAlO_3)_{0.29}(SrTa_{1/2}Al_{1/2}O_3)_{0.71}$ (LSAT(101)) substrates, which provide asymmetric biaxial compressive strains. PFM and (scanning) transmission electron microscopy ((S)TEM) observations indicate periodic stripe ferroelectric 90° domains are formed in these PTO films, with the domain wall lying on $(\bar{1}01)$ of PTO, whose piezoresponse amplitudes have a difference with a critical thickness effect. Moreover, statistical data reveal that the domain width W of this periodic stripe 90° domain and film thickness d have a square root dependent relationship ($W \propto d^{1/2}$). Atomically resolved STEM imaging demonstrates that the stripe 90° domains consist of both wide and narrow c domains with a "head-to-tail" polarization configuration.

2. EXPERIMENTAL SECTION

The PTO thin films with thicknesses ranging from 35 to 70 nm were grown on single-crystal LSAT(101) substrates by pulsed laser deposition, using a KrF excimer laser (λ = 248 nm). The sintered PTO ceramic target with 3 mol % Pb enrichment was used for films

DOI: 10.1021/acsami.8b07206
ACS Appl. Mater. Interfaces 2018, 10, 24627−24637

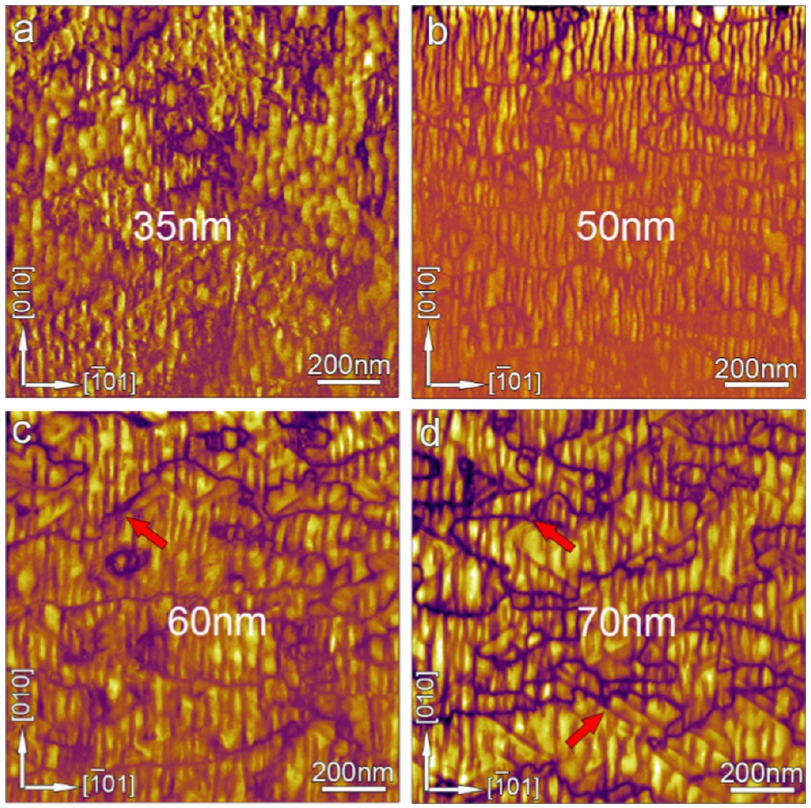

Figure 2. In-plane PFM amplitude images of PTO films on LSAT(101) substrates with different thicknesses: (a) 35 nm; (b) 50 nm; (c) 60 nm; and (d) 70 nm. The vertical stripe domains appear clearly in 50, 60, and 70 nm thick PTO films and indistinctly in 35 nm thick PTO films.

deposition. Before films deposition, the LSAT(101) substrate was heated to 800 °C for 5 min to clean the substrate surface and then cooled down to 700 °C to grow the PTO films. The PTO target was presputtered for 5 min. During deposition, an oxygen pressure of 10 Pa, laser energy density of 2 J cm^{-2}, and a repetition rate of 4 Hz were used. After deposition, the films were annealed at 700 °C for 5 min in an oxygen pressure of 3×10^4 Pa and then cooled down to room temperature (cooling rate ~5 °C min^{-1}).

Surface morphology and piezoresponse force microscopy (PFM) measurements were completed in a scanning probe microscope (Cypher, Asylum Research) using the dual AC resonance tracking mode. Conductive silicon cantilevers with Ti/Ir coating (Asylum Research, Asyelec-01-R) were used for PFM imaging and PFM hysteresis loop measurements. The tip radius is 25 ± 10 nm and the force constant is ≈2.8 N m^{-1}.

Cross-sectional TEM samples were prepared by slicing, gluing, mechanical grinding, dimpling, and finally ion milling. A Precision Ion Polishing System 691 of Gatan company was used for ion milling. Before ion milling, the samples were dimpled down to 10 μm. During milling, a voltage of 5 kV and angles of 7° were used at first. Then, the angles were gradually reduced to 4.5°. The final voltage of milling was less than 0.5 kV for 10 min to clean samples. Plane-view TEM samples were mechanically grinded, dimpled, and ion-milled only from the substrate side.

Bright-field and dark-field images were acquired by Tecnai G^2 F30 transmission electron microscope (TEM). Selected area electron diffraction (SAED) patterns were recorded using JEOL 2100 microscope. All high-angle annular dark-field (HAADF) STEM images were recorded using Titan G^2 60−300 kV microscope with a high-brightness field-emission gun, double aberration (C_s) correctors from CEOS, and a monochromator operating at 300 kV. The beam convergence angle was 25 mrad. Strain analysis was based on geometry phase analysis (GPA), carried out using Gatan Digital Micrograph software.[22,23] Determination of the positions of atoms in the atomic-resolution STEM images was based on Matlab software by two-dimensional Gaussian peak fittings.[17,22]

3. RESULTS

At room temperature, the ferroelectric PTO crystal has a tetragonal structure (space group: $P4mm$) with lattice parameters of $a = b = 0.390$ nm and $c = 0.415$ nm,[37] whereas the LSAT crystal has a cubic structure (space group: $Fm\bar{3}m$) with lattice parameters of $a = b = c = 0.3868$ nm.[38] The LSAT(101) surface has two different in-plane crystal axes: [010] and [$\bar{1}$01], which are different from those of the commonly used LSAT(001) substrate.

The surface topographies of [101]PTO thin films with thicknesses of 35, 50, 60, and 70 nm are shown in Figure 1a−d, respectively. They reveal that the surface root-mean-square (RMS) roughnesses of these PTO films are 1.273, 0.786, 1.700, and 1.897 nm, respectively. It is noted that the 50 nm thick PTO thin film has a smooth surface with a minimum RMS roughness. Besides, the surface structures have an evolution from stripes in both 35 and 50 nm thick PTO films to bulk in both 60 and 70 nm thick PTO films, which indicates a possible domain structure difference within these films. For [101]PTO films with different thicknesses, the phase hysteresis loops in Figure 1e show a well-defined square loop feature, and the amplitude hysteresis loops in Figure 1f display a typical "butterfly shape", suggesting the existence of ferroelectric switch behavior in these PTO thin films.[39,40] Importantly, the 50 nm thick PTO film has a maximum piezoresponse amplitude compared with the rest three PTO films, showing a higher piezoelectric response. It is noted that the 35 nm thick PTO film has a very low piezoresponse

DOI: 10.1021/acsami.8b07206
ACS Appl. Mater. Interfaces 2018, 10, 24627−24637

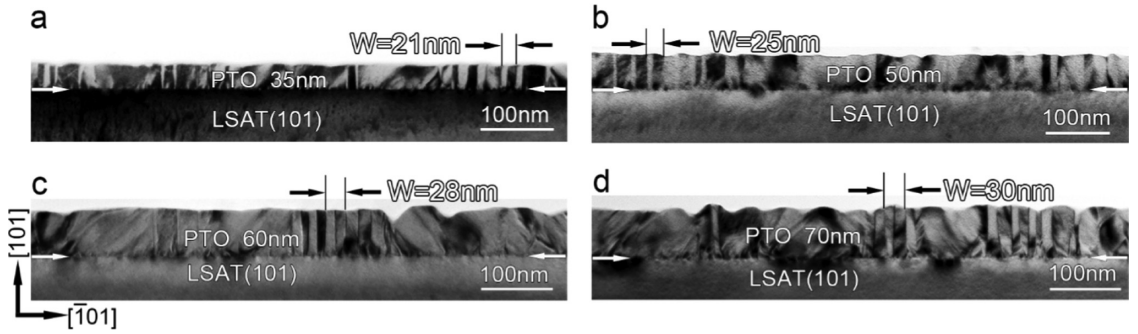

Figure 3. Cross-sectional bright-field TEM images of PTO thin films with different thicknesses grown on LSAT(101) substrates: (a) 35 nm; (b) 50 nm; (c) 60 nm; and (d) 70 nm. The PTO/LSAT(101) interface is denoted by a pair of opposite white arrows. *W* denotes the width of the stripe-like domain.

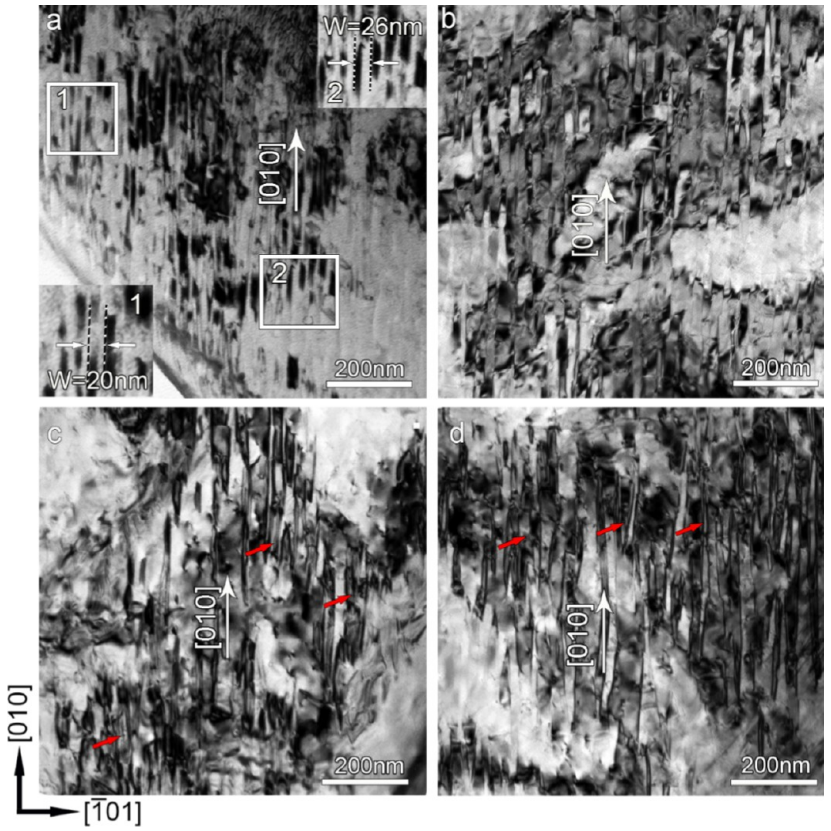

Figure 4. Plane-view TEM images of PTO films on LSAT(101) substrates: (a) 35 nm; (b) 50 nm; (c) 60 nm; and (d) 70 nm. The insets 1 and 2 are enlarged areas labeled as 1 and 2 by white boxes in (a). The red arrows in (c, d) point out the indistinct and overlapped domains.

amplitude, showing a thickness-dependent evolution of piezoelectric response with a critical thickness effect.

Figure 2 shows the in-plane PFM amplitude images of [101]PTO films with different thicknesses, taken with the cantilever's long and scan axes along [010] and [$\bar{1}$01], respectively. Basically, the vertical stripe-like contrast with domain walls lying along [010] axis is observed clearly in 50, 60, and 70 nm thick PTO films, as shown in Figure 2b–d, respectively. It is seen that the width of stripe domains increases with the increasing PTO film thickness. Besides, a few stripe-like contrast with domain walls lying along the ⟨111⟩ axis appears in 60 and 70 nm thick PTO films, as shown in Figure 2c,d (labeled as red arrows), which should be *a*/*c* 90° domains as reported previously.[33] Because the *a*/*c* domain patterns have been studied extensively before, in this article, we focus on the vertical stripe domains, which have drawn less attention previously.

To identify the fine structure of stripe domains, TEM observations were carried out. Figure 3 shows the cross-sectional TEM bright-field images of the [101]PTO films along the in-plane [010] direction. The PTO/LSAT(101) interface is denoted by a pair of opposite white arrows. Some stripe domains with alternate bright and dark contrast can be seen in the PTO film. The domain width (*W*) of about 21 nm is identified in the 35 nm [101]PTO film. In general, the domain structures are very similar in these films with different thicknesses. It is noted that the width of these stripe domains increases from 21 to 25, to 28 nm and finally to 30 nm when the thickness increases from 35 to 50, to 60, and to 70 nm. The domain walls between these domains are very sharp and almost

DOI: 10.1021/acsami.8b07206
ACS Appl. Mater. Interfaces 2018, 10, 24627−24637

perpendicular to the PTO/LSAT(101) interface. Possible misfit dislocations can be identified at the PTO/LSAT(101) interface appearing as many dark dots contrasts. Besides, some inclined and indistinct domains can be seen in these PTO thin films, which are a/c domain patterns and consistent with the PFM measuring results (Figure 2).

For a more general concern, plane-view TEM imaging was further performed. The plane-view bright-field images of PTO films with different thicknesses are shown in Figure 4. In Figure 4a, it is easily seen that the long stripe domains evolve along [010] with alternately bright and dark contrasts. The insets "1" and "2" are enlarged areas labeled as 1 and 2 by white boxes. The width (W) of stripe domains with bright and dark contrast measured in 35 nm thick PTO film ranges within 18−26 nm. With increasing film thickness, the stripe domains are obviously broadened, as shown in Figure 4b−d. Furthermore, the stripe domains are indistinct and overlapped, especially in the 60 and 70 nm thick films, as pointed out by red arrows in Figure 4c,d. It is noted that during the TEM observations of the plane-view samples, the stripe domains appear clearly only when the sample is tilted at a large angle (about 30°) away from the in-plane [010] zone axis of PTO. It is probably because the stripe domains with bright and dark contrast have almost the same diffraction condition when observed from the in-plane direction. Thus, these bright-field images in Figure 4 are obtained under very large tilt angle away from the [010] zone axis for contrast enhancement, which results in the overlapping of stripe domains. However, on this condition, the a/c domain patterns cannot be seen clearly, so only the stripe domains are observed distinctly in the plane-view samples.

To further deduce the relationship of the domain width (W) of periodic stripe domains and the film thickness (d), the data of domain width measured from all the samples with different thicknesses are shown in Figure 5. All the points in Figure 5 are extracted based on the data obtained from a number of bright-field images of cross-sectional samples. Every point represents an average value of domain width from many periodic stripe domains. The formulas $y = ax^b$ and $y = ax + b$ are applied in data fitting by using Origin 8.5 software. The former is curve fit and the latter is linear fit. For $y = ax^b$, the fitting results are a = 3.353 and b = 0.517 with standard errors of 0.876 and 0.065, respectively, which have residual sum of squares of 93.2. For $y = ax + b$, the fitting results are a = 0.257 and b = 12.250 with standard errors of 0.031 and 1.785, respectively, having residual sum of squares of 98.5. The curve fit of $y = ax^b$ shows a relatively small residual sum of squares. Thus, the curve fit is more appropriate. Furthermore, it is easy to see that the value of b is close to 0.5. As shown in Figure 4, the statistical experimental data indicating the relationship between domain width (W) of periodic stripe domains and film thickness are fitted to a curve marked by red solid line, which agrees well with the classical Kittel's law ($W \propto d^{1/2}$) in ferroics as marked by the black dotted line.

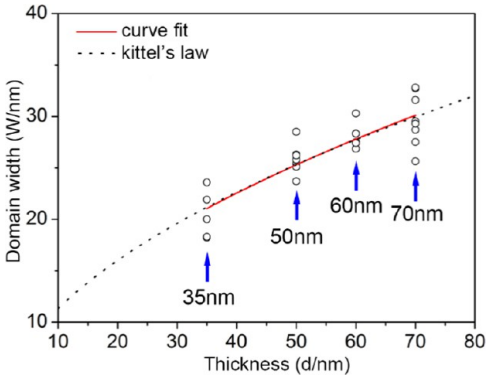

Figure 5. Domain width (W) of periodic stripe-like c_1/c_2 domains as a function of film thickness (d) for (101)-orientated PTO thin films grown on LSAT(101) substrates. The curve fit is close to Kittel's law ($W \propto d^{1/2}$).

To accurately analyze the stripe domains, electron diffraction and contrast analysis were preformed on cross-sectional TEM samples. Figure 6a is a selected area electron diffraction (SAED) pattern taken along the [010]-zone axis of the 50 nm thick PTO film. Figure 6b,c are the enlarged areas of out-of-plane (202) diffraction spots (labeled as 1) and in-plane ($\bar{2}02$) diffraction spots (labeled as 2) in Figure 6a, respectively. It is seen that the out-of-plane (202) diffraction spots split into three spots, whereas the in-plane ($\bar{2}02$) diffraction spots split into two spots. For LSAT substrate, $d_{110} = d_{101} = 0.274$ nm. For PTO, $d_{110} = 0.276$ nm and $d_{101} = 0.284$ nm. The relationship of $d_{101}^{LSAT} \approx d_{110}^{PTO} < d_{101}^{PTO}$ can be acquired. Thus, in Figure 6b, the above spot can be indexed as 202 of LSAT, whereas the other two spots are 202 and 022 of PTO, respectively. Furthermore, the angle of 202 and 022 diffraction spots of PTO can be measured to be about 6.5° (Figure 6a). Similarly, the in-plane diffraction spots are indexed in Figure 6c. Figure 6d,e are two-beam dark-field images taken by different reflections of $\mathbf{g} = 101_c$ and $\mathbf{g} = \bar{1}01_c$, respectively, where the subscript "c" denotes cubic LSAT substrate. In the TEM observation, ferroelectric domains appear as bright contrast in dark-field images, satisfying $\mathbf{g}\cdot\mathbf{P}_s > 0$ under two-beam condition, where $\mathbf{P}_s$ is the polarization vector.[41−43] Figure 6d, taken by the reflection of $\mathbf{g} = 101_c$, shows periodic stripe domains with alternate bright and dark contrast in the PTO film, indicating that the out-of-plane components of the polarization vector of both bright and dark domains have opposite directions. However, stripe domains disappear in Figure 6e, which was taken by the reflection of $\mathbf{g} = \bar{1}01_c$, indicating that the in-plane components of the polarization vector of both bright and dark domains have the same direction. Thus, possible polarization configurations (labeled by yellow arrows) of the stripe domains can be deduced in Figure 6f. To distinguish from a/c domains as well as a_1/a_2 domains in (001)-oriented PTO films, these stripe domains can be named as 90° c_1/c_2 domains (c_1/c_2 domains), which belong to ferroelastic domains.

To further reveal the atomic structures of periodic stripe 90° c_1/c_2 domains, atomic resolution HAADF-STEM images were acquired by aberration-corrected scanning transmission electron microscopy (STEM), which is a very useful tool for studying complex oxides, especially perovskite ferroelectric materials. Figure 7a is a low-magnification high-resolution HAADF-STEM image of the 50 nm thick PTO film, which was recorded along in-plane [010] axis of LSAT. A pair of opposite white arrows denote the PTO/LSAT(101) interface, where some misfit dislocations appear. The blue dotted lines denote the c_1/c_2 domain walls that lie on ($\bar{1}01$). It is pointed out that the c_1/c_2 domains actually consist of both wide and narrow domains, which correspond to the bright and dark contrast areas in Figure 3b. Figure 7b is a magnified HAADF-STEM image corresponding to the red dashed rectangular area in Figure 7a, showing details of the c_1/c_2 domain and domain wall

DOI: 10.1021/acsami.8b07206
ACS Appl. Mater. Interfaces 2018, 10, 24627−24637

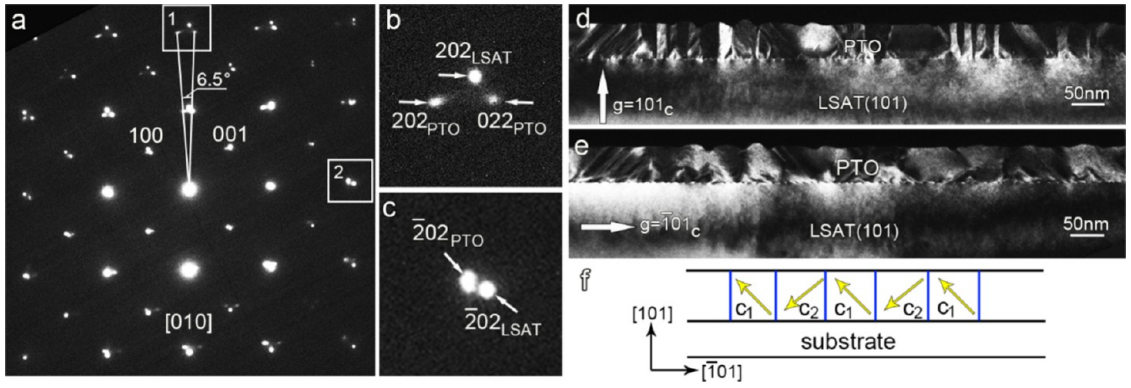

Figure 6. Selected area electron diffraction (SAED) patterns and contrast analysis along [010] zone axis of stripe domain structures in 50 nm thick PTO films on LSAT(101) substrates. (a) SAED pattern taken from the area including the substrate and stripe domains. (b, c) Magnified diffraction spots of white boxes labeled as 1 and 2 in (a). (d) Two-beam dark-field image obtained near the [010] zone axis of LSAT taken by $\mathbf{g} = 101_c$. (e) Two-beam dark-field image obtained near the [010] zone axis of LSAT taken by $\mathbf{g} = \bar{1}01_c$. Note the stripe domain structure disappears when the direction of $\mathbf{g}$ is along the in-plane. (f) Schematic of stripe domain structures. Note the stripe domains can be called 90° c_1/c_2 domains.

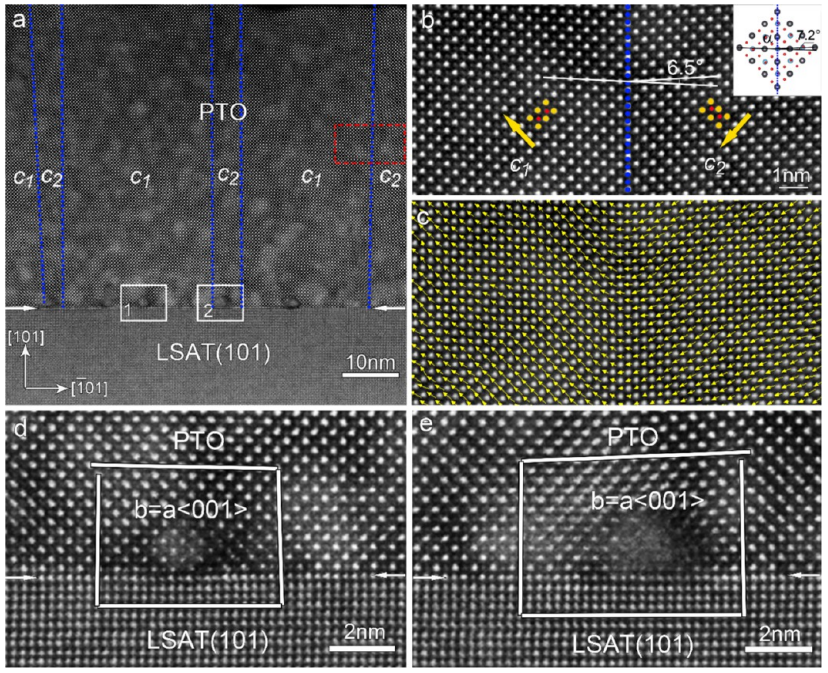

Figure 7. (a) Low-magnification high-resolution HAADF-STEM image showing 90° c_1/c_2 domain in 50 nm thick PTO thin film. The blue dotted lines denote 90° c_1/c_2 domain walls. (b) Atomic-resolution HAADF-STEM image corresponding to the red dashed rectangular box in (a). The blue dotted line denotes 90° c_1/c_2 domain wall. The yellow arrows denote the polarization directions, which are opposite to the displacement of Ti, with [100] for c_1 domains and $[00\bar{1}]$ for c_2 domains. Yellow and red circles denote Pb and Ti atoms, respectively. Note a large lattice rotation with an angle of 6.5° on the right side of 90° c_1/c_2 domain wall. The inset is an atomic schematic model of 90° c_1/c_2 domain wall. (c) Superposition of reversed δ_{Ti} vectors with the experimental image. Yellow arrows denote reversed δ_{Ti} vectors, which are consistent with the spontaneous polarization directions of PTO. (d, e) Atomic-resolution HAADF-STEM images corresponding to two white rectangular boxes labeled as 1 and 2 in (a), which show the misfit dislocations at PTO/LSAT(101) interface.

in atomic resolution. Yellow and red circles denote the positions of Pb and Ti atom columns, respectively (Pb atom column is bright, whereas the Ti atom column is weak based on the HAADF-STEM imaging due to their atomic numbers of heavy Pb (82) and light Ti (22) atoms[22,23,44,45]). Two yellow arrows denote the $\mathbf{P}_s$ directions of the c_1/c_2 domains, which are opposite to the displacements of Ti atoms (δ_{Ti}). The polarization directions are determined to be along [100] for c_1 domains, but $[00\bar{1}]$ for c_2 domains. Lattice rotation with an angle of 6.5° was measured across the 90° domain wall. The inset is an atomic schematic model of the 90° c_1/c_2 domain wall showing a lattice rotation of about 7.2° calculated based on the bulk lattice parameters of tetragonal PTO. Figure 7c shows the corresponding mapping of reversed δ_{Ti} vectors. Yellow arrows denote reversed δ_{Ti} vectors, which are consistent with the spontaneous polarization directions in each PTO unit cells. Figure 7d,e are atomic-resolution HAADF-STEM images corresponding to two white rectangular boxes labeled as 1 and 2 in Figure 7a, showing two interfacial misfit dislocations. By drawing Burgers circuits, it is easily seen that the misfit dislocations have the projected Burgers vectors of $b = a\langle 001\rangle$ on (010) plane.

The strain distribution of periodic stripe c_1/c_2 domains corresponding to the area of Figure 7a is extracted by GPA and

DOI: 10.1021/acsami.8b07206
ACS Appl. Mater. Interfaces 2018, 10, 24627−24637

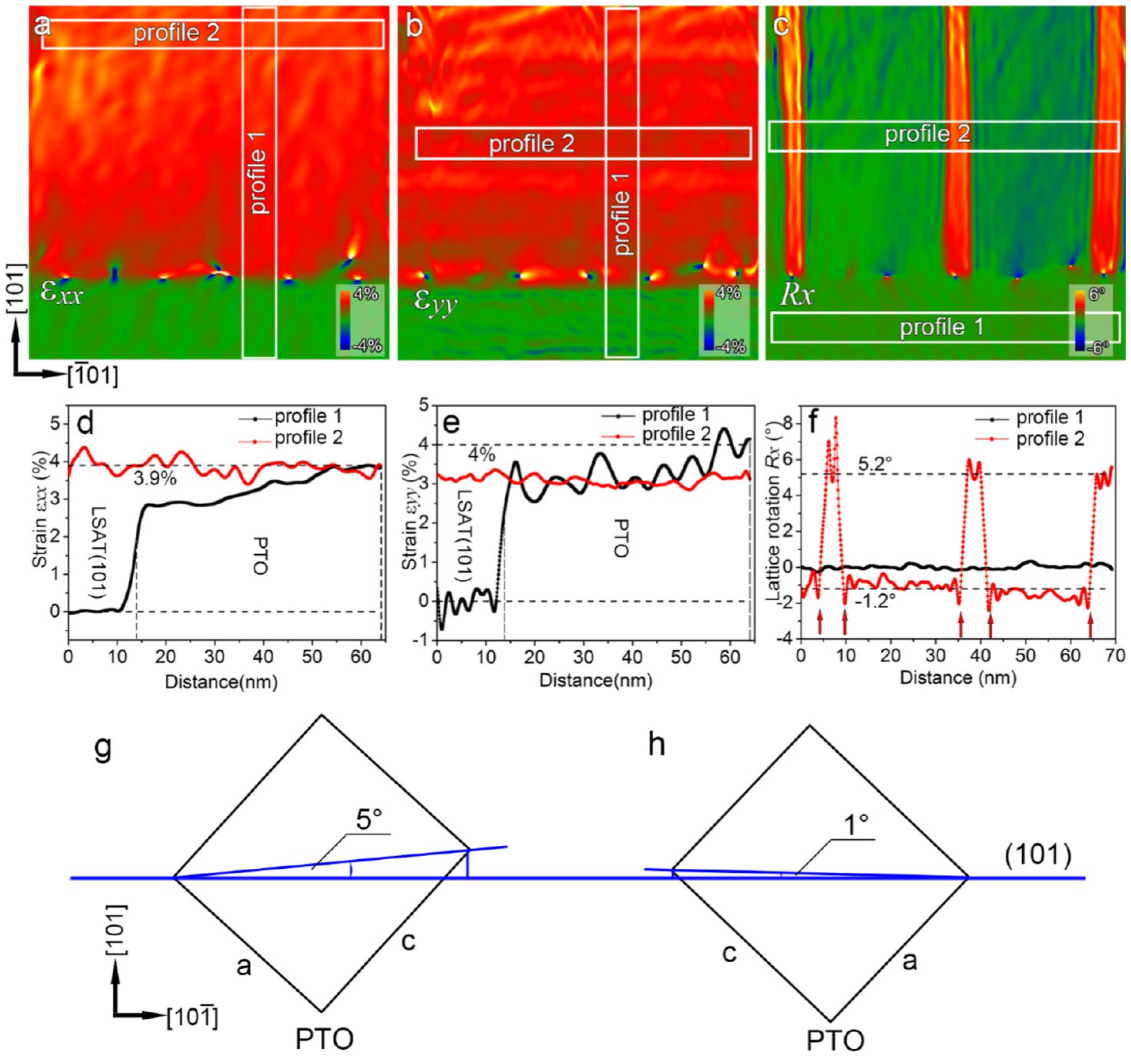

Figure 8. GPA of Figure 7a. (a) In-plane strain (ε_{xx}), (b) out-of-plane strain (ε_{yy}), and (c) lattice rotation (R_x), respectively. Note in (a) and (b), no obvious contrast difference on two sides of 90° c_1/c_2 domain walls exists, whereas obvious contrast difference can be seen on the two sides of 90° c_1/c_2 domain walls in (c). Two line profiles corresponding to two white boxes in (a) are shown in (d). Note no obvious strain difference on two sides of 90° c_1/c_2 domain walls exists. Similarly, two line profiles corresponding to two white boxes in (b) are shown in (e) and two line profiles corresponding to two white boxes in (c) are shown in (f). Note the obvious lattice rotation with an angle of 6.4° on sides of 90° c_1/c_2 domain walls. (g, h) Schematic of in-plane $(10\bar{1})$ spacing projections of PTO showing small rotation angles of c_1/c_2 domains.

shown in Figure 8. Figure 8a–c shows the in-plane strain (ε_{xx}), out-of-plane strain (ε_{yy}), and lattice rotation (R_x), respectively. From Figure 8a,b, it is seen that high-density misfit dislocations can be observed at the interface of PTO and LSAT(101), which is believed to relax the misfit strains of this thin-film system efficiently. From Figure 8c, obvious contrast difference between c_1 and c_2 domains can be observed, indicating that a large lattice rotation exists across the 90° domain wall. Two line profiles labeled as "profile 1" and "profile 2" in Figure 8a, respectively, are shown in Figure 8d. Profile 1 (marked by black solid line) shows the strain variations from the substrate to the film. Compared with the LSAT(101) substrate, the in-plane strain of PTO films jumps at the interface and reaches the value of about 3.9%, which is consistent with the mismatch of 4.1% between the [101]PTO film and LSAT(101) substrate. It is noted that no obvious in-plane strain fluctuations can be identified across the c_1/c_2 domain walls as deduced from profile 2 (marked by red solid line). Similarly, two line profiles of the out-of-plane strain (labeled as profile 1 and profile 2 in Figure 8b, respectively) are shown in Figure 8e, indicating that the out-of-plane strain saturates at about 4.0% at the surface of the PTO film. From Figure 8c, it is pointed out that lattice rotation is significant across the c_1/c_2 domain walls with the angle of about 6° despite the uniform strain distribution across the domain walls. Figure 8f shows two line profiles of the in-plane lattice rotation. A relative lattice rotation angle of ~6.4° across the c_1/c_2 domain walls can be identified, which agrees well with the value measured in Figure 7b.

4. DISCUSSION

In ferroelectric films, domain structures can be widely tuned by film thickness, misfit strain from the substrate, electrical boundary conditions, etc.[16,29,30,46,47] For the present PTO/LSAT(101) thin film system, the lattice mismatch values of the in-plane [010] and [$\bar{1}$01] directions can be calculated by the following formulas[33]

$$\delta(010) = \frac{a_s - a_f}{a_s} \times 100\% \quad (1)$$

DOI: 10.1021/acsami.8b07206
ACS Appl. Mater. Interfaces 2018, 10, 24627−24637

and

$$\delta(\bar{1}01) = \frac{\sqrt{2}\,a_s - \sqrt{({a_f}^2 + c_f^2)}}{\sqrt{2}\,a_s} \times 100\% \quad (2)$$

where subscripts "s" and "f" denote the LSAT substrate and the PTO film, respectively. Therefore, the mismatch strain values calculated along the [010] and [$\bar{1}$01] directions are −0.8 and −4.1%, respectively, which represent asymmetric biaxial compressive strains. Previous studies show that the compressive strain can favor out-of-plane polarized domains.[27] On the one hand, although misfit dislocations evolve at the PTO/LSAT(101) interfaces (Figure 8a), the PTO film near the interface is still not fully relaxed because of the gradual relaxation as shown in Figure 8d, which promotes the formation of c domains with out-of-plane components of polarization vectors, such as the present c_1/c_2 domains. On the other hand, the stability of domain structures in ferroelectric films also depends on the electrostatic boundary conditions.[46,47] If the film has a uniform out-of-plane polarization, it will bring a large depolarization field, which could be reduced or screened by free charges from metallic electrodes,[46] adsorbed ions,[48] ionic point defects on the ferroelectric film surface,[49] reduction of ferroelectric polarization,[50] polarization rotation toward in-plane direction,[51] or by formation of domains with inverse out-of-plane components of polarization vectors.[48,52] In the present work, the formation of alternating c_1/c_2 domains exhibiting alternate upward and downward $\mathbf{P}_s$ (Figure 6f) reduces the depolarization field in PTO films, which is similar to the formation of 109° domains in (001)-oriented $BiFeO_3$ films.[53] Our experiment results are also consistent with previous theoretical calculations that c_1 and c_2 domains with out-of-plane components of polarization vectors are stable under large compressive strains.[51]

According to Kittel's law, periodic stripe domain width is determined by the competition between the energy of the domains E_d and the energy of the domain walls E_w. The former is proportional to domain width W, the later is proportional to d/W, where d denotes the film thickness. Minimizing the total energy of domains and domain walls in the film, the famous square root dependence $W \propto d^{1/2}$ can be deduced.[54] Originally, this square root dependence was deduced in ferromagnets and then extended for ferroelectrics, ferroelastics, and magnetoelectric multiferroics.[54,55] However, the domain walls may be broadened near the electrically open surfaces due to surface charge accumulation, which leads to the deviation of Kittel's law between the domain width W and the film thickness d as reported for (001)-oriented perovskite ferroelectric thin films.[56−58] But, in our work, it is seen that the domain walls are very sharp and thin from the high-resolution HAADF-STEM images. It is also probable that the head-to-tail polarization configuration of the special stripe 90° c_1/c_2 domains can screen the depolarized field and neutralize the surface charges. Thus, the relationship between periodic stripe 90° domain width W and film thickness d in (101)-oriented ferroelectric PTO thin films agrees well with this square root dependence (Figure 5).

Meanwhile, the width of stripe domains reduces when the film thickness decreases, which results in higher density of domain walls. As in previous studies, the high density of domain walls can boost the response to the applied electric field of the films.[31,32] But in our work, we found the thickness-dependent evolution of piezoresponse amplitude with a critical thickness effect. The 50 nm thick PTO film shows a maximum piezoresponse amplitude. It is probably that the domain width (W) of stripe 90° c_1/c_2 domains increase with the film thickness following Kittel's law. The 50 nm thick PTO thin film has a higher density of 90° domain walls than the 60 and 70 nm thick PTO thin films, which leads to the higher piezoresponse of this PTO film. Furthermore, the presence of a/c domains may deteriorate the piezoresponses in 60 and 70 nm thick PTO films. Although the 35 nm thick PTO film may have a higher domain wall density compared with 50 nm thick PTO film, a large number of interfacial misfit dislocations appear due to possibly special island growth mode for the (101)-oriented PTO films form, which results in the very low piezoelectric response in this PTO film.[59]

In addition, it is worth noting that an in-plane lattice rotation with about 6.5° across the 90° c_1/c_2 domain wall is identified in Figure 7b. The in-plane lattice rotation angle is attributed to the large c/a ratio of tetragonal PTO crystal. In a bulk tetragonal PTO unit cell, the crystallographic planes of (101) and ($\bar{1}$01) have an intersection angle that is given by[18,20,60]

$$\alpha = 2\arctan(a/c) \quad (3)$$

The relative angle should be 86.4° for a fully relaxed PTO, so the calculated value of the lattice rotation angle on the two sides of 90° c_1/c_2 domain wall should be 7.2° (Figure 7b). Here, the angle 6.5° is a little smaller than the bulk value, which may be ascribed to the constraints by the substrates. Similar phenomena have been reported on 90° a/c domain and 90° a_1/a_2 domain of (001)-oriented PTO films previously.[20,60]

At last, the special strain distribution in the stripe 90° c_1/c_2 domains should be discussed. Particularly, there is no obvious strain difference in c_1/c_2 domains as shown in Figure 8a,b. The reason may lie in the small rotation angle. From Figure 8g, a rotation of 5° yields a ($\bar{1}$01) spacing projection of cos(5°) $d_{PTO(101)}$ = 0.284 nm × cos(5°) ≈ 0.283 nm, which corresponds to the narrow domain in Figure 8f. In Figure 8h, a rotation of 1° yields a ($\bar{1}$01) spacing projection of cos(5°) $d_{PTO(101)}$ = 0.284 nm × cos(1°) ≈ 0.284 nm, which corresponds to the wide domain in Figure 8f. It is evident that these two values and the corresponding values in the bulk PTO ($\bar{1}$01) spacing of 0.284 nm are actually very close. The maximum change in the in-plane ($\bar{1}$01) spacing induced by the rotation angle of 5° can be calculated as 1 − cos(5°) ≈ 0.38%, which is very small. This result indicates that the misfit strain relaxation through the lattice rotation could hardly complete in the present [101]PTO films. Instead, a large number of misfit dislocations with Burgers vectors of $b = a\langle 001\rangle$ appear at the PTO/LSAT(101) interfaces. The theoretical spacings (S) of these misfit dislocations along [$\bar{1}$01] can be calculated by the following formula[61]

$$S = \frac{b}{f} \quad (4)$$

where b is the magnitude of the projected Burgers vectors on the (010) plane of dislocations and f is the lattice misfit value along [$\bar{1}$01] between the stress-free thin film and substrate. S was calculated to be about 7 nm. Experimentally, the average dislocation spacing (D) between adjacent dislocations was measured from cross-sectional high-resolution HAADF-STEM images to be about 11 nm. Then, the contribution extent (R) of misfit dislocations can be calculated as $R = S/D \approx 64\%$.[61]

DOI: 10.1021/acsami.8b07206
ACS Appl. Mater. Interfaces 2018, 10, 24627−24637

Thus, the formation of the misfit dislocations is a main way to relax the mismatch in these thin-film systems.

5. CONCLUSIONS

In this study, by means of PFM and (S)TEM analysis, we have investigated the periodic stripe ferroelectric 90° c_1/c_2 domain structures, especially the details of these domains and domain walls in (101)-oriented ferroelectric PTO thin films with different thicknesses grown on LSAT(101) substrates. We found that the stripe 90° c_1/c_2 domain width is proportional to the square root of the PTO film thickness, which agrees well with Kittel's law. PFM and STEM analysis reveals that the 50 nm thick PTO films show superior piezoresponse behavior with high density of periodically distributed stripe 90° domains. The stripe 90° domains have an alternate arrangement of wide c_1 and narrow c_2 domains with polarization directions along [100] and [00$\bar{1}$], respectively, forming a head-to-tail polarization configuration. Moreover, the stripe 90° domains have uniform strain distribution and distinct lattice rotations with an angle of 6.5° around the domain walls, decreasing a little, ascribed to the constraints by the substrates. It is proposed that there is a critical thickness about 50 nm showing superior piezoresponse properties, below and above which the films show relatively low piezoresponses due to the existence of interfacial defects, a/c domains or low density of stripe 90° domains. This work can not only help us better understand the domain structures in the (101)-oriented PTO thin films but also demonstrate that proper substrate orientation can be used to modulate domain structures in ferroelectric thin films for potential applications.

AUTHOR INFORMATION

Corresponding Author

*E-mail: ylzhu@imr.ac.cn.

ORCID

Yinlian Zhu: 0000-0002-0356-3306

Author Contributions

Y.Z. and X.M. conceived the project of interfacial characterization in oxides by using aberration-corrected STEM. Y.F., Y.Z., and X.M. designed the experiments. Y.F. performed the thin-film growth and STEM observations. Y.T., D.M., M.Z., M.H., and J.M. participated in the thin-film growth and STEM imaging. All the authors contributed to the discussions and manuscript preparation.

Notes

The authors declare no competing financial interest.

ACKNOWLEDGMENTS

This work is supported by the National Natural Science Foundation of China (Nos. 51571197, 51501194, and 51671194), National Basic Research Program of China (2014CB921002), and the Key Research Program of Frontier Sciences CAS (QYZDJ-SSW-JSC010). Y.T. acknowledges the IMR SYNL-T. S. Kê Research Fellowship and the Youth Innovation Promotion Association CAS (No. 2016177). We are grateful to B. Wu and L. X. Yang of this laboratory for their technical support on the Titan platform of G^2 60−300 kV aberration-corrected scanning transmission electron microscope.

REFERENCES

(1) Scott, J. F. Applications of modern ferroelectrics. *Science* **2007**, *315*, 954−959.

(2) Tsymbal, E. Y.; Gruverman, A.; Garcia, V.; Bibes, M.; Barthélémy, A. Ferroelectric and multiferroic tunnel junctions. *MRS Bull.* **2012**, *37*, 138−143.

(3) Martin, L. W.; Rappe, A. M. Thin-film ferroelectric materials and their applications. *Nat. Rev. Mater.* **2016**, *2*, No. 16087.

(4) Setter, N.; Damjanovic, D.; Eng, L.; Fox, G.; Gevorgian, S.; Hong, S.; Kingon, A.; Kohlstedt, H.; Park, N. Y.; Stephenson, G. B.; Stolitchnov, I.; Taganstev, A. K.; Taylor, D. V.; Yamada, T.; Streiffer, S. Ferroelectric thin films: Review of materials, properties, and applications. *J. Appl. Phys.* **2006**, *100*, No. 051606.

(5) Martin, L. W.; Chu, Y. H.; Ramesh, R. Advances in the growth and characterization of magnetic, ferroelectric, and multiferroic oxide thin films. *Mater. Sci. Eng., R* **2010**, *68*, 89−133.

(6) Tagantsev, A. K.; Cross, L. E.; Fousek, J. *Domains in Ferroic Crystals and Thin Films*; Springer: New York, 2010.

(7) Bratkovsky, A. M.; Levanyuk, A. P. Very large dielectric response of thin ferroelectric films with the dead layers. *Phys. Rev. B* **2001**, *63*, No. 132103.

(8) Zubko, P.; Jecklin, N.; Stucki, N.; Lichtensteiger, C.; Rispens, G.; Triscone, J. M. Ferroelectric Domains in $PbTiO_3$/$SrTiO_3$Superlattices. *Ferroelectrics* **2012**, *433*, 127−137.

(9) Nagarajan, V.; Roytburd, A.; Stanishevsky, A.; Prasertchoung, S.; Zhao, T.; Chen, L.; Melngailis, J.; Auciello, O.; Ramesh, R. Dynamics of ferroelastic domains in ferroelectric thin films. *Nat. Mater.* **2003**, *2*, 43−47.

(10) Ma, Z.; Zavaliche, F.; Chen, L.; Ouyang, J.; Melngailis, J.; Roytburd, A. L.; Vaithyanathan, V.; Schlom, D. G.; Zhao, T.; Ramesh, R. Effect of 90° domain movement on the piezoelectric response of patterned $PbZr_{0.2}Ti_{0.8}O_3/SrTiO_3$/Si heterostructures. *Appl. Phys. Lett.* **2005**, *87*, No. 072907.

(11) Seidel, J.; Martin, L. W.; He, Q.; Zhan, Q.; Chu, Y. H.; Rother, A.; Hawkridge, M. E.; Maksymovych, P.; Yu, P.; Gajek, M.; Balke, N.; Kalinin, S. V.; Gemming, S.; Wang, F.; Catalan, G.; Scott, J. F.; Spaldin, N. A.; Orenstein, J.; Ramesh, R. Conduction at domain walls in oxide multiferroics. *Nat. Mater.* **2009**, *8*, 229−234.

(12) Rojac, T.; Bencan, A.; Drazic, G.; Sakamoto, N.; Ursic, H.; Jancar, B.; Tavcar, G.; Makarovic, M.; Walker, J.; Malic, B.; Damjanovic, D. Domain-wall conduction in ferroelectric $BiFeO_3$ controlled by accumulation of charged defects. *Nat. Mater.* **2017**, *16*, 322−327.

(13) Wei, X. K.; Sluka, T.; Fraygola, B.; Feigl, L.; Du, H.; Jin, L.; Jia, C. L.; Setter, N. Controlled Charging of Ferroelastic Domain Walls in Oxide Ferroelectrics. *ACS Appl. Mater. Interfaces* **2017**, *9*, 6539−6546.

(14) Bhatnagar, A.; Roy Chaudhuri, A.; Heon Kim, Y.; Hesse, D.; Alexe, M. Role of domain walls in the abnormal photovoltaic effect in $BiFeO_3$. *Nat. Commun.* **2013**, *4*, No. 2835.

(15) Yang, M. M.; Bhatnagar, A.; Luo, Z. D.; Alexe, M. Enhancement of Local Photovoltaic Current at Ferroelectric Domain Walls in $BiFeO_3$. *Sci. Rep.* **2017**, *7*, No. 43070.

(16) Li, Y. L.; Hu, S. Y.; Liu, Z. K.; Chen, L. Q. Effect of substrate constraint on the stability and evolution of ferroelectric domain structures in thin films. *Acta Mater.* **2002**, *50*, 395−411.

(17) Jia, C. L.; Mi, S. B.; Urban, K.; Vrejoiu, I.; Alexe, M.; Hesse, D. Atomic-scale study of electric dipoles near charged and uncharged domain walls in ferroelectric films. *Nat. Mater.* **2008**, *7*, 57−61.

(18) Yasui, S.; Ehara, Y.; Utsugi, S.; Nakajima, M.; Funakubo, H.; Gruverman, A. Complex domain structure in relaxed $PbTiO_3$ thick films grown on (100)$_c$$SrRuO_3$//(100)$SrTiO_3$ substrates. *J. Appl. Phys.* **2012**, *112*, No. 052001.

(19) Damodaran, A. R.; Pandya, S.; Agar, J. C.; Cao, Y.; Vasudevan, R. K.; Xu, R.; Saremi, S.; Li, Q.; Kim, J.; McCarter, M. R.; Dedon, L. R.; Angsten, T.; Balke, N.; Jesse, S.; Asta, M.; Kalinin, S. V.; Martin, L. W. Three-State Ferroelastic Switching and Large Electromechanical Responses in $PbTiO_3$ Thin Films. *Adv. Mater.* **2017**, *29*, No. 1702069.

DOI: 10.1021/acsami.8b07206
ACS Appl. Mater. Interfaces 2018, 10, 24627−24637

(20) Li, S.; Zhu, Y. L.; Tang, Y. L.; Liu, Y.; Zhang, S. R.; Wang, Y. J.; Ma, X. L. Thickness-dependent a_1/a_2 domain evolution in ferroelectric $PbTiO_3$ films. *Acta Mater.* **2017**, *131*, 123−130.
(21) Jia, C.-L.; Urban, K. W.; Alexe, M.; Hesse, D.; Vrejoiu, I. Direct Observation of Continuous Electric Dipole Rotation in Flux-Closure Domains in Ferroelectric $Pb(Zr,Ti)O_3$. *Science* **2011**, *331*, 1420−1423.
(22) Tang, Y. L.; Zhu, Y. L.; Ma, X. L.; Borisevich, A. Y.; Morozovska, A. N.; Eliseev, E. A.; Wang, W. Y.; Wang, Y. J.; Xu, Y. B.; Zhang, Z. D.; Pennycook, S. J. Ferroelectrics. Observation of a periodic array of flux-closure quadrants in strained ferroelectric $PbTiO_3$ films. *Science* **2015**, *348*, 547−551.
(23) Liu, Y.; Wang, Y. J.; Zhu, Y. L.; Lei, C. H.; Tang, Y. L.; Li, S.; Zhang, S. R.; Li, J.; Ma, X. L. Large Scale Two-Dimensional Flux-Closure Domain Arrays in Oxide Multilayers and Their Controlled Growth. *Nano Lett.* **2017**, *17*, 7258−7266.
(24) Zhang, Q.; Xie, L.; Liu, G.; Prokhorenko, S.; Nahas, Y.; Pan, X.; Bellaiche, L.; Gruverman, A.; Valanoor, N. Nanoscale Bubble Domains and Topological Transitions in Ultrathin Ferroelectric Films. *Adv. Mater.* **2017**, *29*, No. 1702375.
(25) Yadav, A. K.; Nelson, C. T.; Hsu, S. L.; Hong, Z.; Clarkson, J. D.; Schleputz, C. M.; Damodaran, A. R.; Shafer, P.; Arenholz, E.; Dedon, L. R.; Chen, D.; Vishwanath, A.; Minor, A. M.; Chen, L. Q.; Scott, J. F.; Martin, L. W.; Ramesh, R. Observation of polar vortices in oxide superlattices. *Nature* **2016**, *530*, 198−201.
(26) Damodaran, A. R.; Clarkson, J. D.; Hong, Z.; Liu, H.; Yadav, A. K.; Nelson, C. T.; Hsu, S. L.; McCarter, M. R.; Park, K. D.; Kravtsov, V.; Farhan, A.; Dong, Y.; Cai, Z.; Zhou, H.; Aguado-Puente, P.; Garcia-Fernandez, P.; Iniguez, J.; Junquera, J.; Scholl, A.; Raschke, M. B.; Chen, L. Q.; Fong, D. D.; Ramesh, R.; Martin, L. W. Phase coexistence and electric-field control of toroidal order in oxide superlattices. *Nat. Mater.* **2017**, *16*, 1003−1009.
(27) Zhang, S.; Zhu, Y. L.; Tang, Y. L.; Liu, Y.; Li, S.; Han, M. J.; Ma, J. Y.; Wu, B.; Chen, Z. H.; Saremi, S.; Ma, X. L. Giant Polarization Sustainability in Ultrathin Ferroelectric Films Stabilized by Charge Transfer. *Adv. Mater.* **2017**, *29*, No. 1703543.
(28) Borodavka, F.; Gregora, I.; Bartasyte, A.; Margueron, S.; Plausinaitiene, V.; Abrutis, A.; Hlinka, J. Ferroelectric nanodomains in epitaxial $PbTiO_3$ films grown on $SmScO_3$ and $TbScO_3$ substrates. *J. Appl. Phys.* **2013**, *113*, No. 187216.
(29) Feigl, L.; Yudin, P.; Stolichnov, I.; Sluka, T.; Shapovalov, K.; Mtebwa, M.; Sandu, C. S.; Wei, X. K.; Tagantsev, A. K.; Setter, N. Controlled stripes of ultrafine ferroelectric domains. *Nat. Commun.* **2014**, *5*, No. 4677.
(30) Nesterov, O.; Matzen, S.; Magen, C.; Vlooswijk, A. H. G.; Catalan, G.; Noheda, B. Thickness scaling of ferroelastic domains in $PbTiO_3$ films on $DyScO_3$. *Appl. Phys. Lett.* **2013**, *103*, No. 142901.
(31) Xu, R.; Karthik, J.; Damodaran, A. R.; Martin, L. W. Stationary domain wall contribution to enhanced ferroelectric susceptibility. *Nat. Commun.* **2014**, *5*, No. 3120.
(32) Xu, R.; Liu, S.; Grinberg, I.; Karthik, J.; Damodaran, A. R.; Rappe, A. M.; Martin, L. W. Ferroelectric polarization reversal via successive ferroelastic transitions. *Nat. Mater.* **2015**, *14*, 79−86.
(33) Mtebwa, M.; Mazzalai, A.; Sandu, C. S.; Crassous, A.; Setter, N. Engineered *a/c* domain patterns in multilayer (110) epitaxial $Pb(Zr,Ti)O_3$ thin films: Impact on domain compliance and piezoelectric properties. *AIP Adv.* **2016**, *6*, No. 055104.
(34) Feigl, L.; Sluka, T.; McGilly, L. J.; Crassous, A.; Sandu, C. S.; Setter, N. Controlled creation and displacement of charged domain walls in ferroelectric thin films. *Sci. Rep.* **2016**, *6*, No. 31323.
(35) Zhang, W.; Cheng, H.; Yang, Q.; Hu, F.; Ouyang, J. Crystallographic orientation dependent dielectric properties of epitaxial $BaTiO_3$ thin films. *Ceram. Int.* **2016**, *42*, 4400−4405.
(36) Wada, S.; Yako, K.; Kakemoto, H.; Tsurumi, T.; Kiguchi, T. Enhanced piezoelectric properties of barium titanate single crystals with different engineered-domain sizes. *J. Appl. Phys.* **2005**, *98*, No. 014109.
(37) Glazer, A. M.; Mabud, S. A. Powder profile refinement of lead zirconate titanate at several temperatures. II. Pure $PbTiO_3$. *Acta Crystallogr., Sect. B: Struct. Sci., Cryst. Eng. Mater.* **1978**, *34*, 1065−1070.
(38) Mateika, D.; Kohler, H.; Laudan, H.; Volkel, E. Mixed-perovskite substrates for high-Tc superconductors. *J. Cryst. Growth* **1991**, *109*, 447−456.
(39) Peng, J. J.; Song, C.; Cui, B.; Li, F.; Mao, H. J.; Wang, G. Y.; Pan, F. Manipulation of orbital occupancy by ferroelectric polarization in $LaNiO_3/BaTiO_{3-\delta}$ heterostructures. *Appl. Phys. Lett.* **2015**, *107*, No. 182904.
(40) Li, W.; Wang, Y.; Nie, P.; Hu, Q.; Yang, Y.; Yuan, G. Enhanced switching characteristics and piezoelectric response in epitaxial $BiFeO_3$−$TbMnO_3$ thin films. *Phys. B* **2015**, *466*−*467*, 11−15.
(41) Asada, T.; Koyama, Y. Coexistence of ferroelectricity and antiferroelectricity in lead zirconate titanate. *Phys. Rev. B* **2004**, *70*, No. 104105.
(42) Wang, W. Y.; Zhu, Y. L.; Tang, Y. L.; Xu, Y. B.; Liu, Y.; Li, S.; Zhang, S. R.; Wang, Y. J.; Ma, X. L. Large scale arrays of four-state vortex domains in $BiFeO_3$ thin film. *Appl. Phys. Lett.* **2016**, *109*, No. 202904.
(43) Aoyagi, K.; Kiguchi, T.; Ehara, Y.; Yamada, T.; Funakubo, H.; Konno, T. J. Diffraction contrast analysis of 90° and 180° ferroelectric domain structures of $PbTiO_3$ thin films. *Sci. Technol. Adv. Mater.* **2016**, *12*, No. 034403.
(44) Pennycook, S. J.; Jesson, D. E. High-resolution Z-contrast imaging of crystals. *Ultramicroscopy* **1991**, *37*, 14−38.
(45) Tang, Y. L.; Zhu, Y. L.; Ma, X. L. On the benefit of aberration-corrected HAADF-STEM for strain determination and its application to tailoring ferroelectric domain patterns. *Ultramicroscopy* **2016**, *160*, 57−63.
(46) Nelson, C. T.; Winchester, B.; Zhang, Y.; Kim, S. J.; Melville, A.; Adamo, C.; Folkman, C. M.; Baek, S. H.; Eom, C. B.; Schlom, D. G.; Chen, L. Q.; Pan, X. Spontaneous vortex nanodomain arrays at ferroelectric heterointerfaces. *Nano Lett.* **2011**, *11*, 828−834.
(47) Li, S.; Zhu, Y. L.; Wang, Y. J.; Tang, Y. L.; Liu, Y.; Zhang, S. R.; Ma, J. Y.; Ma, X. L. Periodic arrays of flux-closure domains in ferroelectric thin films with oxide electrodes. *Appl. Phys. Lett.* **2017**, *111*, No. 052901.
(48) Fong, D. D.; Kolpak, A. M.; Eastman, J. A.; Streiffer, S. K.; Fuoss, P. H.; Stephenson, G. B.; Thompson, C.; Kim, D. M.; Choi, K. J.; Eom, C. B.; Grinberg, I.; Rappe, A. M. Stabilization of monodomain polarization in ultrathin $PbTiO_3$ films. *Phys. Rev. Lett.* **2006**, *96*, No. 127601.
(49) Chisholm, M. F.; Luo, W.; Oxley, M. P.; Pantelides, S. T.; Lee, H. N. Atomic-scale compensation phenomena at polar interfaces. *Phys. Rev. Lett.* **2010**, *105*, No. 197602.
(50) Lichtensteiger, C.; Triscone, J. M.; Junquera, J.; Ghosez, P. Ferroelectricity and tetragonality in ultrathin $PbTiO_3$ films. *Phys. Rev. Lett.* **2005**, *94*, No. 047603.
(51) Kornev, I.; Fu, H. X.; Bellaiche, L. Ultrathin films of ferroelectric solid solutions under a residual depolarizing field. *Phys. Rev. Lett.* **2004**, *93*, No. 196104.
(52) Fong, D. D.; Stephenson, G. B.; Streiffer, S. K.; Eastman, J. A.; Auciello, O.; Fuoss, P. H.; Thompson, C. Ferroelectricity in ultrathin perovskite films. *Science* **2004**, *304*, 1650−1653.
(53) Huang, C.; Chen, L. Effects of Interfaces on the Structure and Novel Physical Properties in Epitaxial Multiferroic $BiFeO_3$ Ultrathin Films. *Materials* **2014**, *7*, 5403−5426.
(54) Catalan, G.; Seidel, J.; Ramesh, R.; Scott, J. F. Domain wall nanoelectronics. *Rev. Mod. Phys.* **2012**, *84*, 119−156.
(55) Kittel, C. Theory of the Structure of Ferromagnetic Domains in Films and Small Particles. *Phys. Rev.* **1946**, *70*, 965−971.
(56) Eliseev, E. A.; Morozovska, A. N.; Kalinin, S. V.; Li, Y.; Shen, J.; Glinchuk, M. D.; Chen, L.-Q.; Gopalan, V. Surface effect on domain wall width in ferroelectrics. *J. Appl. Phys.* **2009**, *106*, No. 084102.
(57) Eliseev, E. A.; Kalinin, S. V.; Morozovska, A. N. Finite size effects in ferroelectric-semiconductor thin films under open-circuit electric boundary conditions. *J. Appl. Phys.* **2015**, *117*, No. 034102.

DOI: 10.1021/acsami.8b07206
ACS Appl. Mater. Interfaces 2018, 10, 24627−24637

(58) Vorotiahin, I. S.; Eliseev, E. A.; Li, Q.; Kalinin, S. V.; Genenko, Y. A.; Morozovska, A. N. Tuning the polar states of ferroelectric films via surface charges and flexoelectricity. *Acta Mater.* **2017**, *137*, 85−92.
(59) Nagarajan, V.; Jia, C. L.; Kohlstedt, H.; Waser, R.; Misirlioglu, I. B.; Alpay, S. P.; Ramesh, R. Misfit dislocations in nanoscale ferroelectric heterostructures. *Appl. Phys. Lett.* **2005**, *86*, No. 192910.
(60) Catalan, G.; Lubk, A.; Vlooswijk, A. H.; Snoeck, E.; Magen, C.; Janssens, A.; Rispens, G.; Rijnders, G.; Blank, D. H.; Noheda, B. Flexoelectric rotation of polarization in ferroelectric thin films. *Nat. Mater.* **2011**, *10*, 963−967.
(61) Suzuki, T.; Nishi, Y.; Fujimoto, M. Analysis of misfit relaxation in heteroepitaxial $BaTiO_3$ thin films. *Philos. Mag. A* **1999**, *79*, 2461−2483.

DOI: 10.1021/acsami.8b07206
ACS Appl. Mater. Interfaces 2018, 10, 24627−24637